



# Quantifying Uncertainty in Predictions of Spacecraft Erosion Induced by a Hall Thruster

Mackenzie E. Meyer\*<sup>1</sup> and Matthew P. Byrne<sup>†</sup>  
*University of Michigan, Ann Arbor, Michigan 48109*

Iain D. Boyd<sup>‡</sup>  
*University of Colorado Boulder, Boulder, Colorado 80309*  
 and

Benjamin A. Jorns<sup>§</sup>  
*University of Michigan, Ann Arbor, Michigan 48109*

<https://doi.org/10.2514/1.A35196>

**The impact of sputtering yield model uncertainty on the predicted erosion of a meshed reflector wire exposed to a Hall effect thruster plume is investigated. Quantifying this uncertainty is critical for making informed assessments of reflector lifetime. The erosion is modeled by assuming known ion current density and energy distribution at the location of the wire. The wire surface is then discretized, and wear is evaluated incrementally over time. The confidence in model predictions is quantified where the major source of uncertainty is assumed to stem from the material sputtering yield. The model is run to simulate reflector erosion after 10 h of exposure to a 3 kW class Hall thruster operating at 300 V. The simulated results then are compared to experimental measurements from a dedicated wear test performed on a series of mesh coupon samples. The experimental results are shown to fall largely within the 95% credible intervals from model predictions, though the uncertainty in the maximum predicted erosion is found to be up to 190% of the maximum predicted erosion. These results are discussed in the context of predicting lifetime of reflectors on orbit and the need for margin in this component design.**

## I. Introduction

THE Hall effect thruster is a form of in-space propulsion that has a higher propellant efficiency compared to more traditional chemical rockets. This high fuel efficiency, which stems from the ability of these devices to accelerate their propellant to high speeds (greater than 20 km/s), makes the Hall thruster ideally suited for a wide range of applications, such as orbit raising and station keeping, where propellant efficiency is paramount. Yet, while Hall thrusters have been shown to be a reliable technology, there are a number of systems-level challenges with integrating these devices on spacecraft. Most notably, the energetic xenon exhaust of these systems can impinge on and erode surfaces mounted adjacent to the thruster through ion-impact sputtering. Over sufficiently long exposure times, this erosion poses a risk to these nearby components [1–4].

In light of this threat to spacecraft health, there have been a number of studies on the problem of erosion from plume–spacecraft interactions [5–17]. The shared goal of these works, which have been primarily modeling based, has been to determine the erosion of spacecraft surfaces when subject to a thruster plume on orbit. These types of predictions are critical as they inform estimates for spacecraft life limitations due to erosion and strategies for how to place the thruster to mitigate this erosion.

With that said, there is a major potential source of uncertainty in most modeling efforts performed to date that stems from how the sputtering yield (the number of eroded particles per incident ion) of

the material is modeled. This uncertainty can lead to significant variance in prediction for the key erosion processes.

The large uncertainty in the sputtering models stems from the fact that they are primarily semi-empirical. They must be calibrated against data sets where the quality, applicability, and sparsity in the data all contribute to the model uncertainty [18–28]. For example, in many cases, the data employed to calibrate the models are generated under controlled conditions that are not representative of the plume environment. Similarly, many data sets do not extend to the lower energies (less than 100 eV) typical of the peripheries of Hall thruster plumes. To capture the erosion of spacecraft materials, extrapolation thus must be performed based on the model. This can lead to high levels of uncertainty, often multiple orders of magnitude, in the estimated sputtering yield. This effect is compounded by the fact that many sputtering models are highly nonlinear in the lower energy regime [29]. As the rate of erosion of materials scales linearly with the sputtering yield of the material, this uncertainty in principle could translate to low levels of confidence in spacecraft erosion predictions. In light of the critical challenge posed by the plume–spacecraft interaction, there is a pressing need to quantify the impact of this uncertainty on the confidence in model predictions for erosion.

The goal of this study is to assess the role of sputtering yield uncertainty on a recently validated model for the erosion of coated round wires subject to the plume of a xenon-based Hall effect thruster [30,31]. This particular application is motivated by the widespread use of this type of thin wire geometry in communications antennae. This paper is organized in the following way. In the first section, we describe the model, its implementation, and the framework for performing forward uncertainty quantification for erosion predictions. In the second section, following the approach first described by Yim [29] and employed by others [32–34], we apply Bayesian inference to quantify the uncertainty in sputtering yield for the two constituent materials in the coated wire, gold and molybdenum. In the third section, we briefly review the details of the experimental setup and data that were used to validate the model developed in our previous work [30,31]. In the fourth section, we compare the model predictions under uncertainty to experimental data sets. In the fifth and final section, we discuss our results in the context of the limitations of the model and future implications for assessing erosion due to plume–spacecraft interactions.

Presented as Papers 2019-3987 and 2019-3988 at the AIAA Propulsion and Energy 2019 Forum, Indianapolis, IN, August 19–22, 2019; received 29 June 2021; revision received 2 November 2021; accepted for publication 5 November 2021; published online 16 December 2021. Copyright © 2021 by the American Institute of Aeronautics and Astronautics, Inc. All rights reserved. All requests for copying and permission to reprint should be submitted to CCC at [www.copyright.com](http://www.copyright.com); employ the eISSN 1533-6794 to initiate your request. See also AIAA Rights and Permissions [www.aiaa.org/randp](http://www.aiaa.org/randp).

\*Ph.D. Candidate, Applied Physics Program; [maemeyer@umich.edu](mailto:maemeyer@umich.edu) (Corresponding Author).

<sup>†</sup>Ph.D. Candidate, Applied Physics Program.

<sup>‡</sup>H.T. Sears Memorial Professor, Ann and H.J. Smead Aerospace Engineering Sciences.

<sup>§</sup>Assistant Professor, Department of Aerospace Engineering.

## II. Model Description

In the following section, we overview the details of our model for wire erosion and how we assess the role of sputtering yield uncertainty. To this end, we first review the details of how we calculate wire erosion. This is based on the work we presented in Ref. [30]. We then introduce three semi-empirical sputtering yield models that we leverage in our model for the wire. Finally, we discuss how we quantify the confidence in the model predictions due to uncertainty in these sputtering yields.

### A. Erosion Model

We show in Fig. 1 a notional cross-section of the surface geometry we model. This is composed of a rounded wire, typical of what would be employed as an element in an antenna reflector. The wire is composed of a lower substrate of molybdenum with a gold coating. For the case we model, we assume the wire cross-section is initially circular and subject to ion bombardment from one direction ( $-y$  in the figure). As ions impact the surface of this wire, they sputter the material, facilitating the gradual erosion of this surface. This process is shown notionally in Fig. 1.

To capture this process quantitatively, we leverage the erosion model we developed and validated in our previous work [30]. We briefly describe its major features here. The cross-section of the wire is discretized into 200 planar surfaces. Over a small, differential piece of time, the erosion depth  $\Delta h$  of each surface then can be written as

$$\Delta h = \frac{j_i m_m}{q \rho_m} \Delta t \int Y(E, \theta) f_i(E) dE \quad (1)$$

where  $j_i$  is the ion current density,  $q$  is the fundamental charge,  $m_m$  is the atomic mass of the sputtered target material,  $\rho_m$  is the density of the target material,  $\Delta t$  is the time step that varies from 1 to 10 s,  $Y(E, \theta)$  is the combined sputtering yield (atoms removed per incident ion) that depends on the ion energy  $E$  and angle of incidence  $\theta$ , and  $f_i(E)$  is the ion energy distribution. The ion energy distribution is normalized so the integral over all energies is unity. We assume the ions impacting the wire are singly charged and incident from the  $-y$  direction. The key inputs the model requires include the wire geometry, material, and the properties of the incident ion flux. As this equation shows, the erosion depth scales linearly with the ion current density and the sputtering yield. Therefore, as the ion current density or sputtering yield increases, the erosion depth also increases.

To simulate the erosion of a wire surface subject to a known plume environment, we advance the profile per Eq. (1) in the following way.

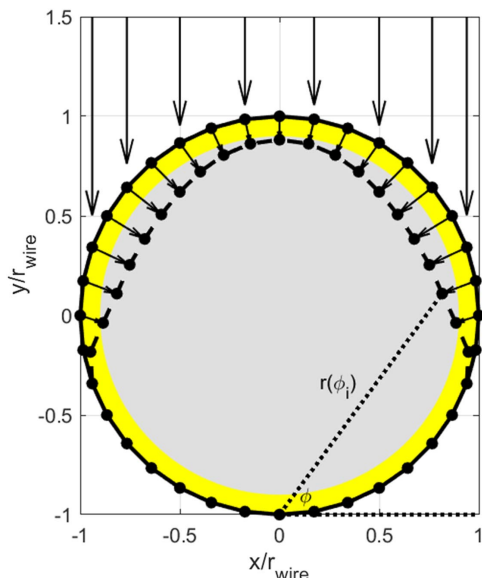


**Fig. 1** Example of erosion from an initial configuration (solid) to eroded profile (dashed) by incident ion flux (black arrows). Notional gold cladding on molybdenum core is shown.

At each time step, we determine the angle of incidence between the incident ion direction (the  $-y$  direction) and the surface normal of each discretized surface. We then determine the material of each segment (gold coating or molybdenum core) by calculating the distance of the midpoint of the surface from the cylinder axis. The material then informs our choice of sputtering yield model (Sec. II.B). Armed with this value, we calculate the erosion depth of the given segment. We then advance the endpoints of each segment by first calculating where each endpoint would move based on the erosion depth of each adjacent surface. We then average these two points to calculate the final endpoint. An example of the endpoint movement is shown in Fig. 1. We repeat this process until the specified simulation end time is reached, the wire has completely eroded, or no additional erosion occurs. When a significant amount of erosion occurs, loops and other unphysical features can form. We remove these unphysical features, as detailed in our previous work [30].

### B. Sputtering Yield Models

There are a number of models for the sputtering yield of typical spacecraft materials subject to ion bombardment [18–20,26,28,35,36]. These depend on both the species of incident particle as well as the sputtered material. In our case, we confine ourselves to sputtering yields for gold and molybdenum, the constituent materials for the wire, with an incident gas of singly charged xenon ions. With this in mind, it is typical for modeling this sputtering process to represent the two dependencies of the yield (energy and angle) as independent,

$$Y(E, \theta) = Y(E)Y(\theta) \quad (2)$$

where the normal incidence model  $Y(E)$  is a function of the incident ion energy and the angular factor  $Y(\theta)$  is a function of the incident angle with respect to surface normal. Both  $Y(E)$  and  $Y(\theta)$  are physics-based semi-empirical models that require model parameters to fit the measured sputtering yields. In our previous work, we found the best agreement with experimentally measured wire profiles when we used the normal incidence model from Eckstein and Preuss and the angular factor from Wei et al. [18,20,30]. In this work, we also consider

the angular factor from Yamamura and Shindo [19] to illustrate how the angular factor affects the predicted eroded wire profiles.

The normal incidence Eckstein and Preuss model is based on the revised Bohdansky [36] formula and is updated to better reflect sputtering by low-energy ions [18]. The form for the energy-dependent sputtering yield is given by

$$Y(E) = Q s_n(\epsilon) \frac{((E/E_{th}) - 1)^\mu}{(\lambda/w) + ((E/E_{th}) - 1)^\mu} \quad (3)$$

where  $Q$ ,  $\lambda$ ,  $\mu$ , and  $E_{th}$  are the model parameters.  $Q$  is a scaling parameter that adjusts the magnitude of the sputtering yield and depends on the incident ion and target material;  $\lambda$  indicates the energy at which the sputtering yield begins to decrease;  $\mu$  represents the exponent in the interatomic potential;  $E_{th}$  is the threshold energy, below which the sputtering yield is zero. The reduced energy  $\epsilon$  is given by

$$\epsilon = E \frac{m_m}{m_i + m_m} \frac{0.03255}{Z_i Z_m \sqrt{Z_i^{2/3} + Z_m^{2/3}}} \quad (4)$$

where  $m_i$  is the atomic mass of xenon,  $m_m$  is the atomic mass of the material being sputtered,  $Z_i$  is the atomic number of xenon,  $Z_m$  is the atomic number of the material being sputtered, and  $E$  is the incident xenon ion energy;  $w$  depends on the reduced energy  $\epsilon$  by

$$w = \epsilon + 0.1728\sqrt{\epsilon} + 0.008\epsilon^{0.1504} \quad (5)$$

The nuclear stopping cross-section  $s_n(\epsilon)$  is based on the krypton-carbon potential

$$s_n(\epsilon) = \frac{0.5 \log(1 + 1.2288\epsilon)}{w} \quad (6)$$

We consider two forms of the angular factor. The first is from Yamamura and Shindo [19],

$$Y(\theta) = \left(\frac{1}{\cos\theta}\right)^f \exp\left(-f \cos\theta_{\text{opt}} \left(\frac{1}{\cos\theta} - 1\right)\right) \quad (7)$$

where  $f$  and  $\theta_{\text{opt}}$  are the model parameters;  $\theta_{\text{opt}}$  is the optimal angle, or the angle where the angular factor and therefore total sputtering yield is maximized. Physically,  $f$  is a model parameter that in principle can depend on the incident ion energy and threshold energy of sputtering [28], but we assume  $f$  is independent of energy for this work.

The second model for the angular factor is from Wei et al. [20,29],

$$Y(\theta) = \frac{1}{\sqrt{1 + (\beta/\alpha)^2 \tan^2\theta}} \exp\left(\frac{1}{2} \left(\frac{a}{\alpha}\right)^2 \left[1 - \frac{1}{1 + (\beta/\alpha)^2 \tan^2\theta}\right]\right) \quad (8)$$

where  $a/\alpha$  and  $\beta/\alpha$  are the model parameters;  $a$  represents the projected energy range,  $\alpha$  is the longitudinal straggling range, and  $\beta$  is the transverse straggling range [29].

### C. Uncertainty Quantification in Model Predictions

There are multiple sources of uncertainty for the erosion model described in the preceding section. These include uncertainty in the model inputs as well as uncertainty in the model parameters in the sputtering yields. However, because we use experimental measurements for the plasma properties which are taken with a high degree of certainty, we assume the dominant source of uncertainty stems from the model parameters,  $\Theta = (\lambda, f, \dots)$  in the sputtering yield models. We represent the uncertainty associated with these parameters by treating them as random variables described by probability distribution  $P(\Theta)$ . Provided we know this distribution of parameters (Sec. III), we can quantify the impact of model uncertainty on the predictions of erosion by random sampling from the distribution and running the model multiple times.

To this end, for a given measured input of ion current density and ion energy distribution, we randomly sample from this distribution of model parameters 10,000 times and apply these values in the erosion model to produce 10,000 unique eroded wire profiles. We correlate these profiles by placing the endpoints from each segment into bins based on angle  $\phi$  from the point  $(0, -r_{\text{wire}})$  and line segment defined by  $y = -r_{\text{wire}}$  and the positive  $x$  direction (convention shown in Fig. 1). As depicted in Fig. 2, the centers of the bins  $\phi$  are chosen based on the angle of the initial points on the discretized surface, and the bounds of the bins are the averages of the two adjacent angles. The inclusivity of the bounds of the bins are chosen to be symmetric around  $\phi = 90$  deg, where the point farthest from  $\phi = 90$  deg is inclusive and the other is exclusive, except at  $\phi = 90$  deg, where both are inclusive. At the edges, the bins are between  $\phi \in [0 \text{ deg}, \frac{\phi_1}{2}]$  and  $\phi \in [\frac{\phi_n + 180 \text{ deg}}{2}, 180 \text{ deg}]$ , where  $\phi_n$  represents the angle of the last point as measured counter-clockwise from  $(0, -r_{\text{wire}})$ .

Once we have binned the 10,000 profiles, we have data sets of the distribution of distance  $r(\phi_i)$  of the endpoints from the point  $(0, -r_{\text{wire}})$  in each bin (convention shown in Fig. 1). From these, we calculate the median ( $r_{50}(\phi_i)$ ), fifth percentile ( $r_5(\phi_i)$ ), and 95th percentile ( $r_{95}(\phi_i)$ ) distances from  $(0, -r_{\text{wire}})$ . These distances are then translated into points,  $(x(\phi_i), y(\phi_i))$  for the  $i$ th bin, by using the angle at the center of the bin. In this way, we are able to create predictions for the median erosion profile and credible intervals based on the variance in the sputtering yield measurements. We also calculate the uncertainty of the erosion by taking the distance between the fifth percentile and median in each bin,  $r_{50}(\phi_i) - r_5(\phi_i)$ , and the distance between the 95th percentile and median in each bin,  $r_{95}(\phi_i) - r_{50}(\phi_i)$ . These values represent the uncertainty of the upper

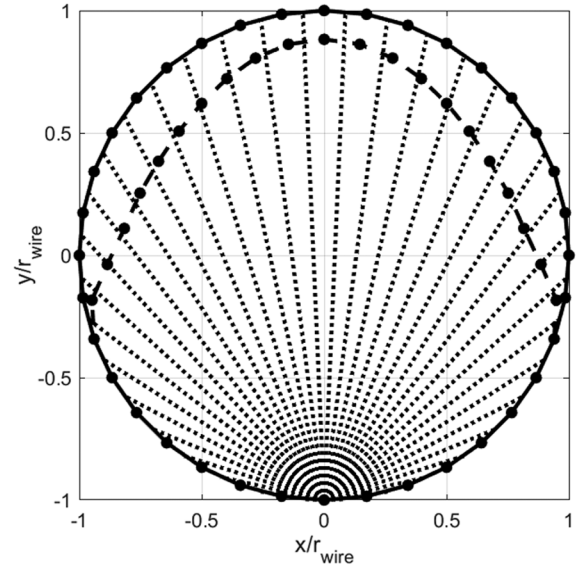


Fig. 2 Points in the final profile (dashed) are sorted into bins based on their angle  $\phi$  from  $(0, -r_{\text{wire}})$  and positive  $x$  values in  $y = -r_{\text{wire}}$ .

and lower limits of erosion, respectively. We determine the erosion depth of the median profile by taking the distance between the median distance and the point on the initial profile in each bin,  $r_{\text{initial}} - r_{50}(\phi_i)$ , where  $r_{\text{initial}}$  is the distance between the initial point in each bin and  $(0, -r_{\text{wire}})$ . We report the maximum erosion of the median profile with + and - margins, where the + value corresponds to the maximum distance between the fifth percentile and median and the - value corresponds to the maximum distance between the 95th percentile and median. Note these maximum quantities are not necessarily found in the same angular bin. We also calculate the relative uncertainty, or the maximum distance between the fifth percentile and median divided by the maximum erosion of the median. This relative uncertainty represents the worst-case scenario of uncertainty in our erosion estimates. To assess convergence with number of samples, we computed the relative uncertainty for varying numbers of samples. We found the relative uncertainty differs by less than 2 percentage points after 6000 samples. Similarly, to calculate the maximum erosion of the experimental measurements, we sort the points in the experimental measurements into the same bins and calculate  $r_{\text{initial}} - r_{\text{exp}}$ , where  $r_{\text{exp}}$  is the distance of the experimental profiles from  $(0, -r_{\text{wire}})$ . We then take the maximum.

### III. Model Parameter Inference for Sputtering Yield Models

As we discussed in Sec. II.B, the models we employ for sputtering are semi-empirical. Thus, while the form of each model is rooted in a physical understanding of the process of sputtering, they must be calibrated against experimental data. The resulting model parameters inferred from this calibration have inherent uncertainty that stems from both variance in the data and the fidelity of the model. We represent this uncertainty in model parameters  $\Theta$  with the characteristic probabilistic distributions  $P(\Theta)$  introduced in Sec. II.C. We describe in this section our method for inferring these distributions from sputtering data sets compiled from previous work. This is based on the same analysis technique used by Yim [29] and is rooted in a Bayesian approach.

Following this Bayesian approach to model inference, we treat the model parameters as random variables where their probability distribution can be inferred from experimental data,

$$P(\Theta) \propto \mathcal{L}(d|\Theta)\pi(\Theta) \quad (9)$$

where  $\pi(\Theta)$  is the joint prior probability distribution of the parameters and  $\mathcal{L}(d|\Theta)$  is the likelihood function of data set  $d$ . The prior

probability distribution is based on a prior belief about the distribution of the parameter. For this work, following the approach of Yim [29], we chose uniform distributions for all model parameters where the possible ranges of each of these distributions are based on previously published parameter fits [18–20,29]. The likelihood function indicates the probability that, assuming the model with fit parameters  $\Theta$  is correct, measurements would yield the data set  $d$ . While it is a common practice to employ a Gaussian distribution for the likelihood, we follow Yim in choosing a likelihood function based on a log-normal distribution,

$$\mathcal{L}(d|\Theta) = \prod_{j=1}^N \frac{1}{\sigma\sqrt{2\pi}} \cdot \exp\left[-\frac{1}{2\sigma^2} \left(\ln\left[\frac{y_j}{M(x_j; \Theta)}\right]\right)^2\right] \quad (10)$$

where  $x_j$  and  $y_j$  are independent and dependent elements, respectively, of the data set  $d$ ,  $N$  is the number of points in the data set,  $M(x; \Theta)$  is the model, and  $\sigma$  is assumed to be 1. We make this assumption due to the high variance in the disparate data sets we used. Because the stated error in these data does not come close to encompassing this variance in the data points, we do not include it in this analysis.

The experimental data we used in the likelihood function were extracted from data sets from several previous sputtering studies [21–28]. These consisted of measurements of both the normal incidence sputtering as a function of energy (Fig. 3) and the angular factor of sputtering (Fig. 4) for xenon ions on both gold and molybdenum. As can be seen, the magnitudes of the reported data can vary significantly depending on the study (cf. Fig. 3b). This underscores the inherent uncertainty in these data that results from variance in the test and testing conditions. With this in mind, we substituted the compiled data sets into Eq. (9) and generated the probability distribution of the model parameters by employing a nested sampling Markov chain Monte Carlo routine [37]. For our analysis of each model, we used 10,000 live points, which are iterated upon approximately 200,000 times. Figure 5 shows a representative result of the probability distributions generated by inferring the parameters from the Eckstein and Preuss normal incidence model for xenon sputtering of molybdenum. The probability distribution in this case is represented in two ways: with joint distributions and marginal distributions. The joint distributions show the partially marginalized probability distribution as a function of two of the model parameters. We have normalized each distribution such that the labeling indicates the total percentage of samples that are contained below the contour. The marginal distributions plot the probability of the single model parameter.

The probability distributions are a graphical indication of the model parameters that best match the data and the relative confidence in these parameters. The peaks in each distribution correspond to the

most probable value for the parameter. The characteristic width of the marginal distributions represents the relative uncertainty in the parameters. This uncertainty ultimately stems from the spread in the experimental data as well as the limited fidelity of the semi-empirical models.

By sampling from these joint distributions, we can represent the impact of parameter uncertainty on the model predictions. By assuming that the most probable model fits are the ones most likely to represent reality, we can propagate the uncertainty in the fits to predict the most likely erosion rates. To this end, we first select one of the elements  $\Theta$  from the joint distribution described previously to evaluate the sputtering yield at each energy (for normal incidence,  $Y(E)$ ) and angle (for the angular factor,  $Y(\theta)$ ). We then repeat this process for all samples to yield a data set of predicted sputtering at the given energy or angle. Figures 3 and 4 show the resulting median of these data sets (solid line) along with fifth and 95th percentiles (dashed lines). To be clear, the credible intervals for sputtering yield are not the variation in expected sputtering yield but are a quantification of our belief that a particular sputtering yield will be observed. In the case of the normal incidence model for molybdenum (Fig. 3a), the median and credible intervals are tightly constrained. This is in large part driven by the availability of data points at the lower incident ion energies where the model is highly nonlinear. This nonlinearity weights the fit to these data points. On the other hand, the model fit to gold (Fig. 3b) exhibits uncertainty exceeding an order of magnitude. This underscores the impact of both the disparity in data sets and the relative sparsity of data where the model is most nonlinear, near the threshold energy for sputtering of approximately 20 eV. As we will see in the next section, this uncertainty can contribute to wide variances in erosion predictions.

For the angular dependence of sputtering yield  $Y(\theta)$  shown in Fig. 4, we see that, while the median lines generally follow the data, the credible intervals extend to ranges on the order of the value of the median. This is a function of the relative sparsity of the data as well as the nonlinearity of the model. The disparity is particularly pronounced for the sputtering of gold where there is only one available data set. With that said, while the credible intervals are relatively large compared to the median, the magnitude in the uncertainty in the angular dependence of sputtering yield is only on the order of unity. We anticipate that this uncertainty thus will have less of an impact on sputtering compared to the larger order of magnitude variance in the normal incidence models.

In summary, we have described in this section the approach for quantifying model uncertainty for the normal incidence and angular dependence models for sputtering. In Sec. V, we again employ sampling methods to investigate how the uncertainty in these sputtering yields impacts confidence in wire erosion predictions. Before

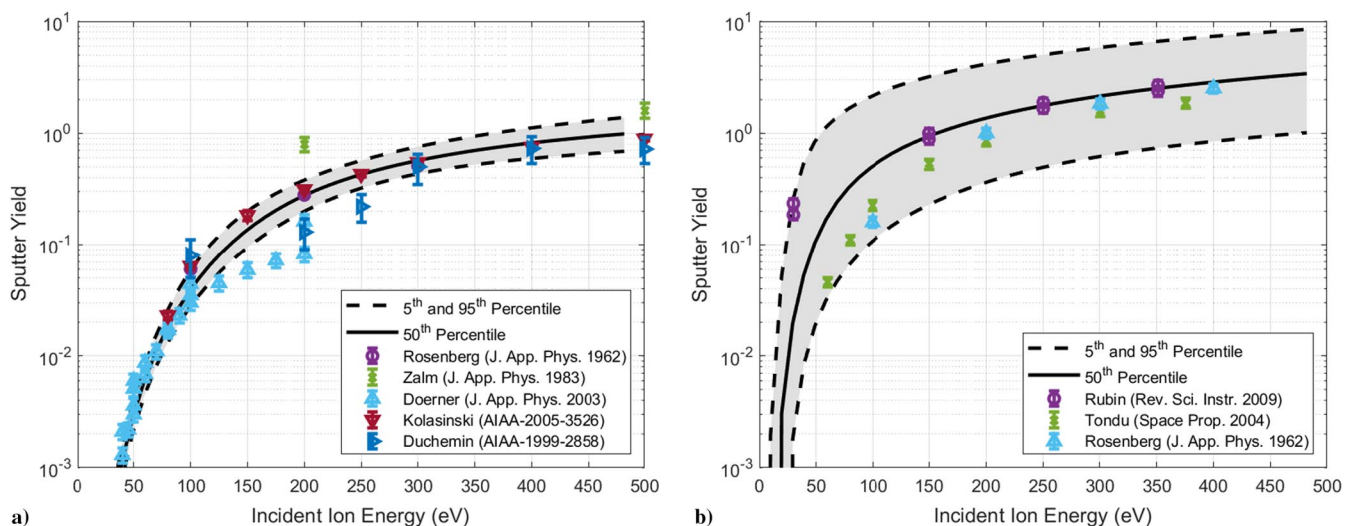
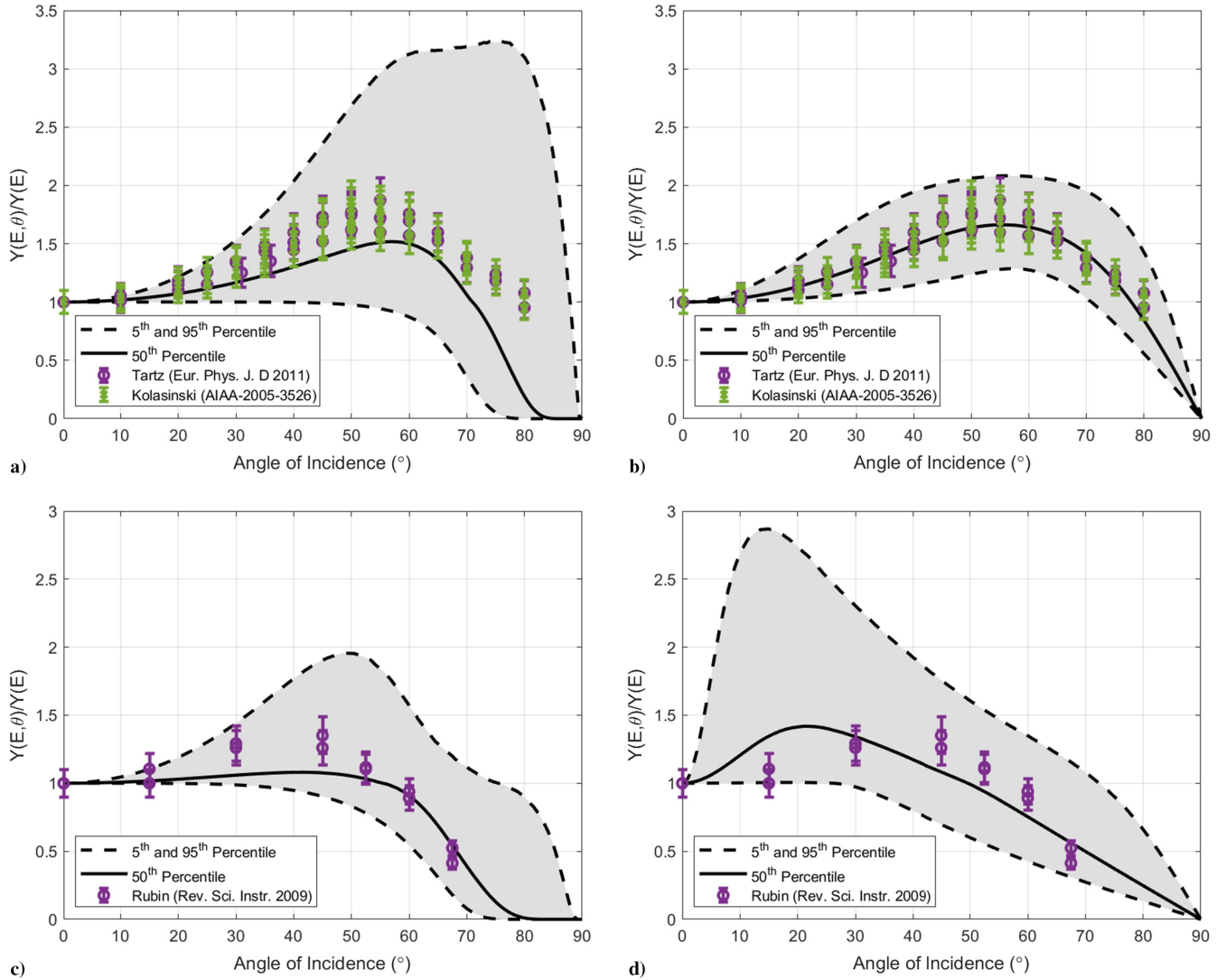


Fig. 3 Experimental data and model fits for normal incidence sputtering yield models for xenon incident on a) molybdenum [21–25] and b) gold [21,26,27].



**Fig. 4** Experimental data and model fits for angular incidence sputtering yield models for xenon incident on molybdenum and gold: a) model from Yamamura and Shindo for molybdenum [24,28], b) model from Wei et al. for molybdenum [24,28], c) model from Yamamura and Shindo for gold [26], and d) model from Wei et al. for gold [26].

proceeding with this analysis, however, we first discuss the experimental measurements we employed for model validation.

#### IV. Experimental Measurements for Model Inputs and Validation

To inform the input conditions for our model as well as validate its predictions, we require experimental measurements of wire erosion in a Hall thruster plume as well as local plasma measurements of the environment near the wire. To this end, we employed data we generated from a previous experimental study. We briefly describe here the nature of the measurements and key findings. Additional details can be found in Ref. [31].

##### A. Test Article and Erosion Measurements

Figure 6 shows the experimental layout from Ref. [31] for performing a controlled erosion study of mesh wire. We employed the H6, 6 kW class Hall thruster [38–42], as the plasma source in this work. This laboratory device (Fig. 6a) was jointly developed by the University of Michigan, the United States Air Force Research Laboratory, and the Jet Propulsion Laboratory. It has a centrally mounted cathode and operates on xenon gas.

We experimentally characterized the erosion of the wire in four mesh reflector coupons placed in the plume of the H6 thruster when operated at a discharge voltage of 300 V and power of 3 kW (Fig. 6b).

These coupons were placed equidistant from one another, 1 m from the thruster, and facing the thruster. The exposure time of 10 h and sample locations were chosen to accelerate the erosion while simultaneously sampling a broad range of plume locations.

We quantified the erosion of these mesh surfaces using a laser confocal microscope. While the mesh coupons include many wires, we chose one wire in the coupon to quantify the erosion. The erosion measurements consisted of the average of profiles taken at five different locations along the wire axis (Fig. 7). The reported experimental measurements and uncertainty represent the average and standard deviation from these five profiles. As we discuss in Ref. [31], due to the structure of our samples, the absolute height of the profile could not be determined from the measurements. In this work, we determine the absolute height by having the most experimentally measured data points fall within the credible intervals of the results of the erosion model.

##### B. Plume Properties

To inform the erosion model predictions (Eq. (1)) for the mesh wire coupons, we used the plasma measurements from Ref. [31] that were taken at the same locations as the wire samples. The generated data included the ion energy distribution  $f_i(E)$ , as inferred with a retarding potential analyzer, and the ion current density  $j_i$ , as measured with a Faraday probe. We have reproduced these results from our previous work [31] in Fig. 8. Figure 8a shows the ion current density as a

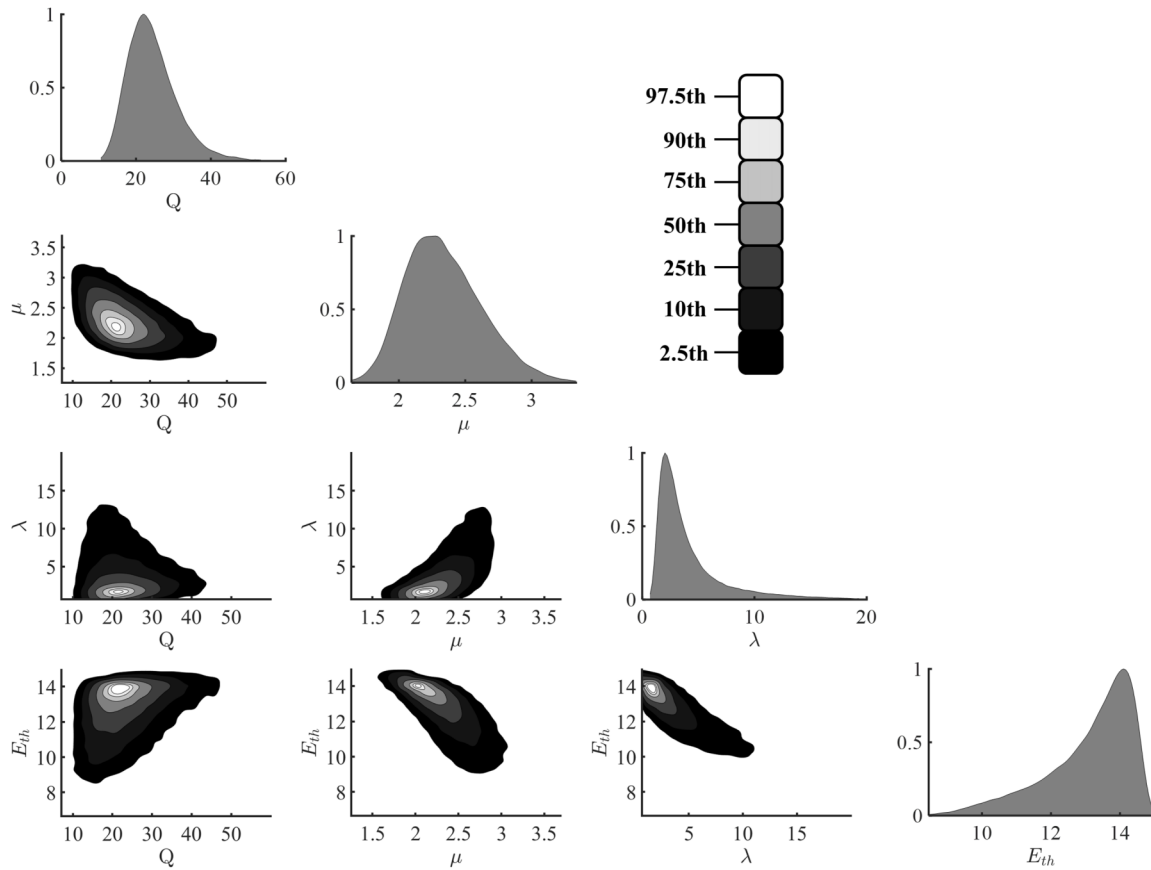
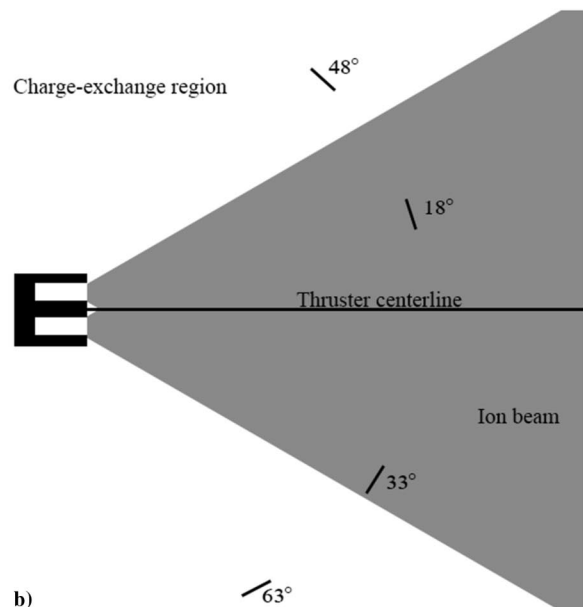


**Fig. 5** Joint and marginal probability distributions for model parameters of the sputtering model from Eckstein and Preuss for molybdenum. Labeling indicates percentage of samples contained below the contour.



a)



b)

**Fig. 6** Experimental setup: a) the H6 6 kW Hall effect thruster, operating at 300 V and 3 kW, during a mesh material wear test [31] in the Large Vacuum Test Facility at the University of Michigan and b) notional layout of sample placement for wire erosion measurements.

function of angle measured from thruster centerline. As can be seen here, the ion current density is at its maximum on the thruster centerline and decreases with angle. This is a typical feature of Hall thruster plumes [43]. Figure 8b shows the ion energy distribution at the four angular locations of the coupons. Near the thruster centerline (18 deg), the energy distribution shows a most probable energy of 280 eV, which is comparable to the discharge voltage. This is

expected for the centerline where the main beam of the exhaust is directed. As the angle from the thruster centerline increases to locations at the periphery of the main beam, the most probable energy decreases in magnitude, and a population starts to grow with a most probable value of 30 eV. This lower-energy population is likely attributed to the formation of charge-exchange ions that result from collisions of the main beam with ambient neutrals. As we discussed

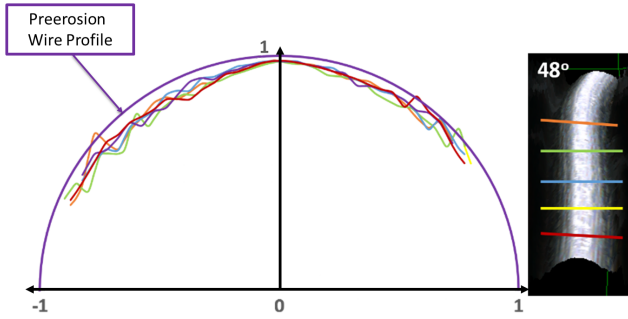


**Fig. 7** Each wire segment is characterized at a series of higher focal planes, producing a three-dimensional map of its surface. Five height profiles were extracted.

and ultimately showed in Ref. [31], the wire samples located closest to the thruster centerline are subject to the highest rates of erosion. This is due to the combination of higher ion energy and flux to the target. The samples farther from centerline experience diminishing levels of erosion. The wide range of erosion rates provides a diverse data set for comparison with the model.

## V. Results

In this section, we present the results of the impact of sputtering model uncertainty on erosion predictions. To this end, we use the erosion model described in Sec. II.A with the experimentally measured plume properties detailed in Sec. IV.B to model the erosion of wires over 10 h of exposure to the plume of the H6 Hall thruster. We sample from the joint probability distributions of model parameters described in Sec. III 10,000 times to generate 10,000 unique eroded wire profiles. We combine these profiles to obtain a median profile with quantified uncertainty as described in Sec. II.C.

We examine the eroded wire profiles at 1 m from the thruster and at four angles from the thruster centerline (18, 33, 48, and 63 deg), shown notionally in Fig. 6b. We use time step of 1 s at 18 deg from the thruster centerline and 10 s at the other three locations. These time steps are based on our convergence study in Ref. [30]. We defined convergence as the difference between locations of endpoints that start at the same location on the wire being less than 1% of a wire radius. Convergence was achieved for 33, 48, and 63 deg from the thruster centerline at a time step of 10 s. While we found convergence at 18 deg required time steps of 0.05 s, taking these time steps would have been prohibitively computationally expensive. Instead, we chose a time step of 1 s, as relatively little variation in the final wire profiles was seen. Figures 9–12 show the eroded wire profiles we

calculated using the previously described model at these four locations. At each location, we include the results for both angular incidence sputtering yield models. For comparison, we also plot the experimentally measured profiles from our previous work [31] and described in Sec. IV.A.

Figure 9 shows the results at 18 deg from the thruster centerline. This location exhibits the highest erosion out of the four coupons because both the ion current density and ion energies are highest at this location. As can be seen, both sputtering models (Wei et al. and Yamamura and Shindo) qualitatively agree with the experimental results. Most notably, they successfully predict a characteristic peak, which (as we discuss in the following section) is due to the preferred erosion that occurs at the optimal angle of the angular incidence sputtering yield. Similarly, the maximum erosion predicted on the median profile is 114% of a wire radius from the Wei et al. model (+49% of a wire radius, -42% of a wire radius) and 94% when we use the model from Yamamura and Shindo (+55% of a wire radius, -35% of a wire radius). This compares favorably to the experimental result which shows over 97% of the experimentally measured profile lies within the credible intervals.

We note that, despite the quantitative and qualitative agreement with data, for both cases, the credible intervals of the models are large compared to the median prediction. This result underscores the large degree of uncertainty that stems from the uncertainty in sputtering yield. Indeed, because the maximum credible intervals are on the order of the maximum erosion, the lifetime of the reflector could be substantially overestimated. We expand upon the implications of this result in the following section.

We show in Fig. 10 results at 33 deg from the thruster centerline. Because of the lower ion current density (Fig. 8a) and lower number of high-energy ions (Fig. 8b), there is less erosion at this location than at 18 deg from the thruster centerline. As with the 18 deg case, the shape of the eroded wire profile differs between the two angular incidence sputtering yield models. More erosion is seen near  $x/r_{\text{wire}} \pm 1$  when we use the model from Wei et al. than when we use the model from Yamamura and Shindo. Quantitatively, the maximum erosion in the median profile is 14% of the wire radius (+7% of a wire radius, -5% of a wire radius) when we use the model from Wei et al. and 13% of the wire radius (+15% of a wire radius, -6% of a wire radius) when we use the model from Yamamura and Shindo. The experimentally measured profile agrees well with the model predictions with over 89% of the experimentally measured profile lying within the credible intervals. With respect to model confidence, the maximum credible intervals are smaller than those at 18 deg. This is ultimately because the wire erodes less in 10 h due to the lower ion current density and less-energetic ions striking the wire. The perhaps more relevant metric, however, is the relative magnitude of the uncertainty, which

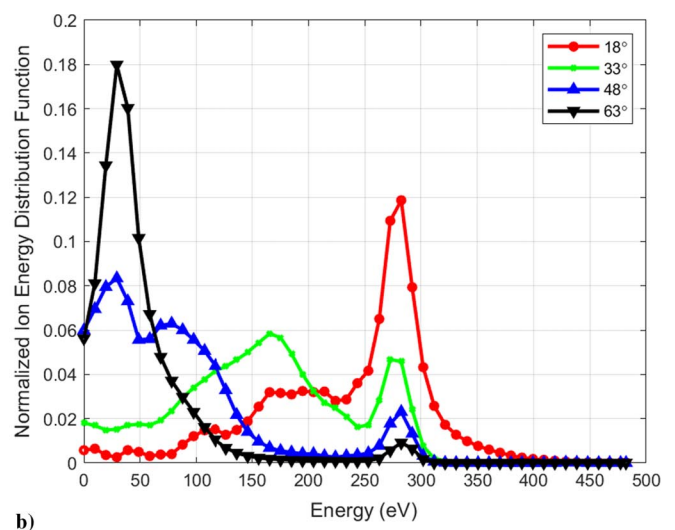
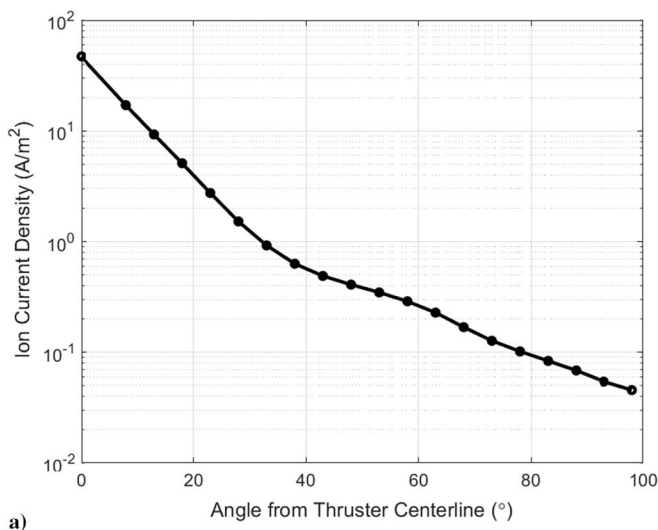


**Fig. 8** Plasma properties: a) ion current density and b) ion energy distributions for the H6 Hall thruster operating at 300 V and 3 kW. Measurements performed at 1 m from thruster. Data from Ref. [31].

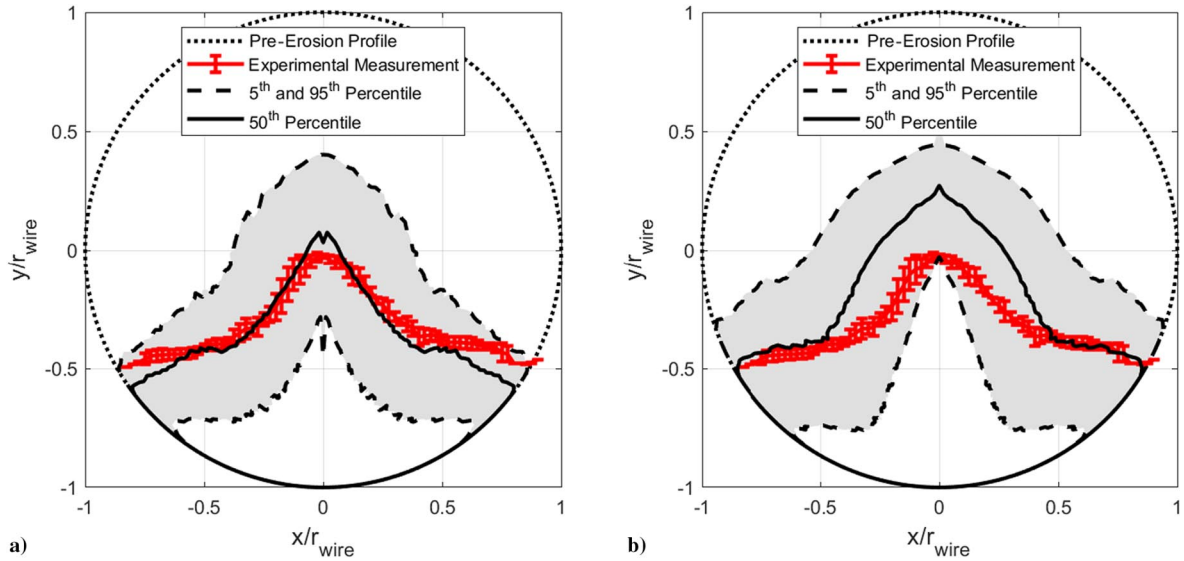


**Fig. 9** Eroded wire profiles at 18 deg from the thruster centerline using the angular incidence model from a) Wei et al. and b) Yamamura and Shindo.

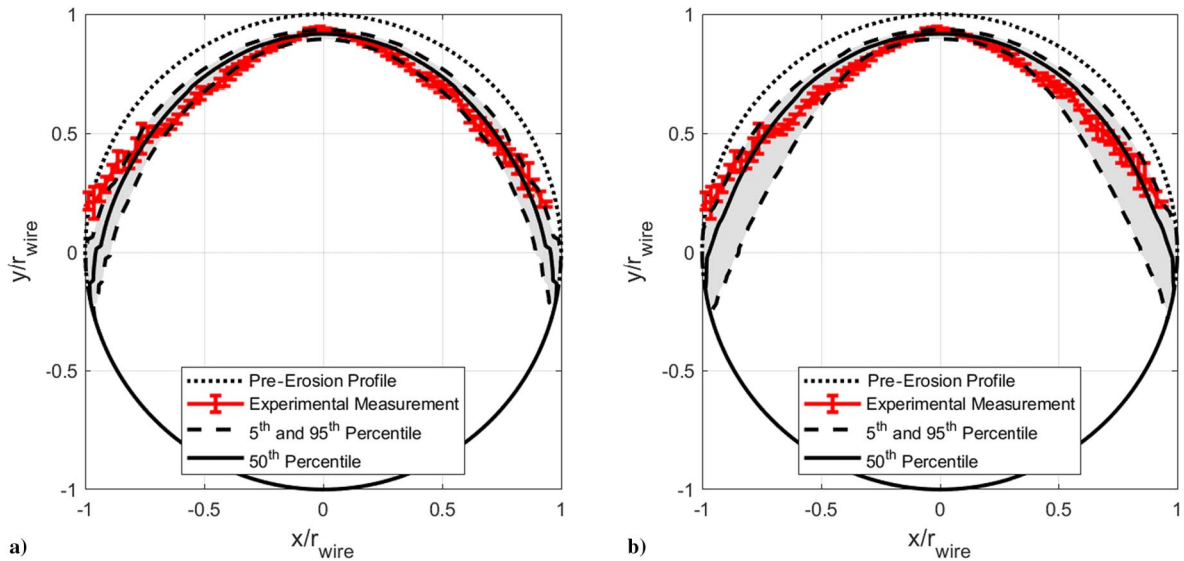


**Fig. 10** Eroded wire profiles at 33 deg from the thruster centerline using the angular incidence model from a) Wei et al. and b) Yamamura and Shindo.

in this case is on the order of the maximum erosion. This result thus illustrates again the driving role of uncertainty in lowering the confidence in the erosion prediction.

Figure 11 shows the results at 48 deg from the thruster centerline. At this location, the ion current density is less than half of the ion current density at 33 deg from the thruster centerline, and the ion energy distribution shows most ions have energies below 150 eV. We therefore predict and measure less erosion here than at 18 and 33 deg from the thruster centerline. The predictions from the two models are qualitatively similar. Quantitatively, the maximum erosion on the wire is 4.1% of the wire radius (+3.5% of a wire radius, -3.3% of a wire radius) when we use the model from Wei et al. and 4.1% of a wire radius (+4.1% of a wire radius, -3.3% of a wire radius) when we use the model from Yamamura and Shindo. Over 74% of the experimentally measured profile lies within the credible intervals. In terms of model confidence, we again note that the credible intervals are smaller in magnitude at 48 deg from the thruster centerline than at 33 deg from the thruster centerline because there is less erosion of the wire overall. However, the maximum credible intervals are approximately the size of the maximum erosion on the median profile, indicating a large relative uncertainty in the erosion prediction.

Figure 12 shows the results at 63 deg from the thruster centerline. This location exhibits the lowest ion current density (less than half of the ion current density at 48 deg from the thruster centerline), and the ion energy distribution shows most of the ions have an energy below 50 eV with the most probable energy at 29 eV. We therefore see the lowest amount of erosion at this location. Indeed, it is barely discernible from the initial wire profile, and the gold coating has not been removed. The maximum erosion on the median profile is 2.0% of a wire radius (+3.3% of a wire radius, -1.5% of a wire radius) and 1.9% of a wire radius (+3.6% of a wire radius, -1.4% of a wire radius) when we use the models from Wei et al. and Yamamura and Shindo, respectively. The predictions of our model again agree quantitatively with the experimentally measured profile, with 85% of the experimentally measured profile falling within the credible intervals. While the absolute value of uncertainty is lower than in the other, higher erosion cases, because the maximum credible interval can be nearly double the maximum erosion on the wire, the relative uncertainty in the erosion is larger for this outermost angle.

For a side-by-side comparison, we combine the results from all four angles in Fig. 13a, in which we plot both the predicted and measured maximum erosion as a function of angle from the thruster

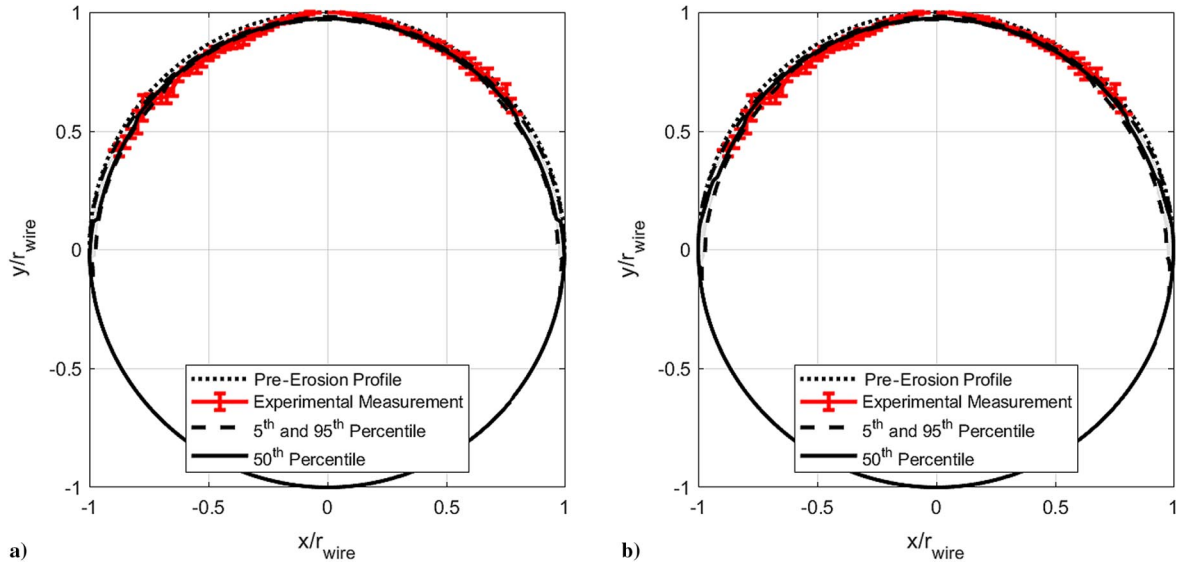


Fig. 11 Eroded wire profiles at 48 deg from the thruster centerline using the angular incidence model from a) Wei et al. and b) Yamamura and Shindo.

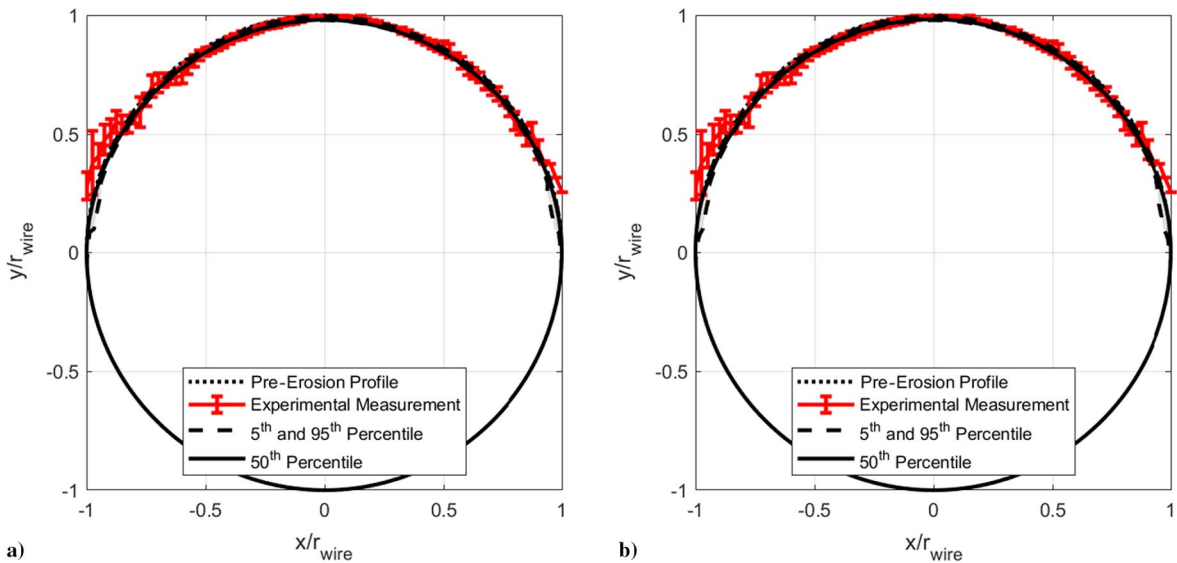


Fig. 12 Eroded wire profiles at 63 deg from the thruster centerline using the angular incidence model from a) Wei et al. and b) Yamamura and Shindo.

centerline. This graphically illustrates how the maximum erosion of the experimental measurements agrees well, within credible intervals, with the maximum erosion of our predictions. Moreover, as we discussed in the preceding, we can see that the maximum erosion decreases with angle from the thruster centerline. This is the result of the decrease in current density and ion energy with increasing angle.

With that said, while the magnitude of the credible intervals for the erosion scales with the magnitude of median erosion, we see (Fig. 13b) that the relative uncertainty (maximum distance between the fifth percentile and median divided by the maximum erosion of the median) does not decrease with angle in the same way. Rather, the relative uncertainty is the lowest at 18 deg from the thruster centerline and generally increases, with the exception of the model from Yamamura and Shindo at 33 deg, with angle from the thruster centerline. This result shows that our prediction for the periphery of the plume has the highest degree of uncertainty; the relative confidence is at least the same magnitude as the value of the median prediction. This is a notable result as it is the location where we actually anticipate spacecraft components will be placed. We discuss potential reasons for why the relative uncertainty is higher at this location in Sec. VI.

In summary, we have shown that when we systematically account for model-based uncertainty, our predictions for the eroded wire profiles match the experimental results within uncertainty. With that

said, the uncertainty in the sputtering yield does have a substantial impact on our confidence in model prediction. Indeed, the maximum credible intervals we calculated yielded variances in the erosion that are on the order of the median predictions. These variances in turn (particularly in the periphery of the plasma) could translate to large uncertainty (up to 190%) in spacecraft component lifetime when exposed to a thruster plume. We further discuss the implications of these results in the following section.

## VI. Discussion

We discuss in this section the implications of our findings. We begin with a comment on the unusual shape of the eroded profiles. We then discuss the implications of our results for assessing lifetime, the role of the uncertainties that we did not assess, the limitations of our model, and recommendations for improving confidence in erosion predictions.

### A. Physical Implications of Erosion Results

As we saw in the previous section, the experimentally measured and predicted eroded wire profiles (Fig. 9) show an unusual structure; they become progressively peaked when subject to more bombardment. This shape is a physical manifestation of the fact that the

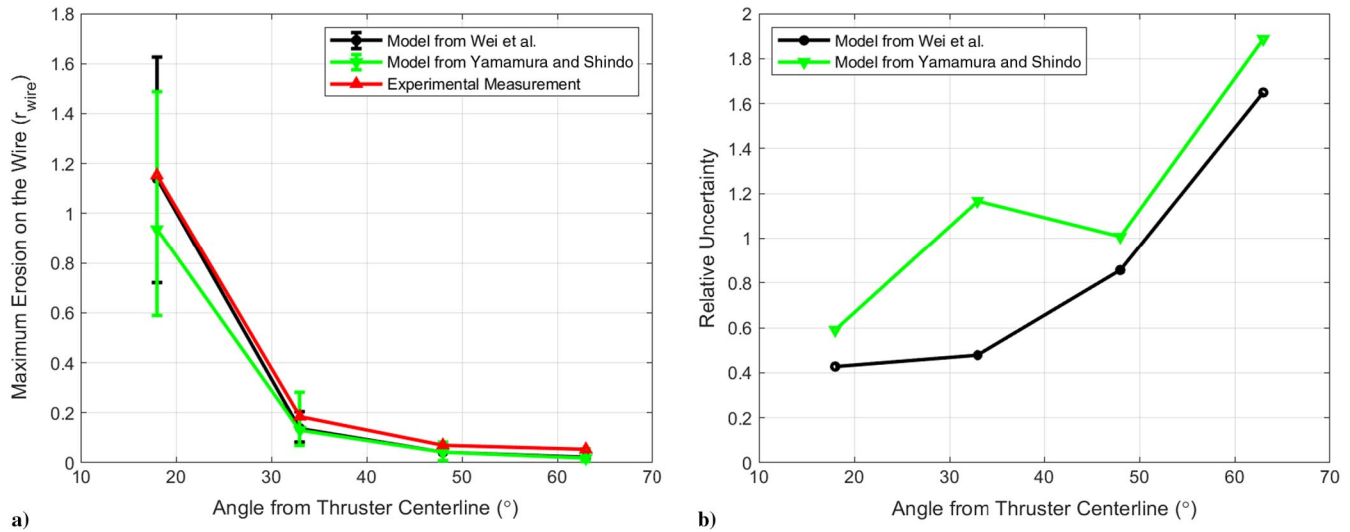


**Fig. 13** Dependence on angle from thruster centerline of a) maximum erosion on the wire (error bars on the model results show the maximum erosion of the fifth and 95th percentile credible intervals) and b) relative uncertainty.

sputtering depends on the angle of incidence between the surface and the incoming ions. As we show in Fig. 4, the optimal angle, or angle where the sputtering yield is maximized, is not at normal incidence (0 deg) but instead is between 20 and 60 deg. In fact, the sputtering yield at the optimal angle can be three times as large as the sputtering yield at normal incidence. Therefore, for the same ion current density and ion energy distribution, a surface at the optimal angle will experience three times the erosion compared to a surface at normal incidence. Because more sputtering occurs at surfaces near the optimal angle, we see more erosion on the wire at locations off axis from the direction of normal beam incidence. This leads to the gradual steepening of the wire profile. This peak is especially pronounced when the wire has been substantially eroded, such as at 18 deg from the thruster centerline (Fig. 9).

Both the model uncertainty and model choice impact the predicted shape of this steepening. As we showed in Sec. III, the uncertainty in the angular sputtering model can lead to wide variance in the predicted optimal angle for erosion. This is captured by the fact that the credible intervals show profiles that exhibit different degrees of steepening in Fig. 9. Moreover, in reviewing the sputtering fits for both the models from Wei et al. and Yamamura and Shindo (Fig. 4), we see that the model from Yamamura and Shindo more rapidly decays to zero at higher angle of incidence. This in turn can explain the more steplike structure exhibited in the predicted erosion from this model (Fig. 9b). Finally, we note that for all the sputtering yield models, particularly the Yamamura and Shindo model in Fig. 4, there is a high degree of uncertainty at oblique angles (greater than 80 deg). This likely contributes to the qualitative disagreement in model predictions at the edges of the wire ( $x = \pm r_{\text{wire}}$ ) in Figs. 9 and 10 where the angle of ion incidence is largest.

### B. Implications of Uncertainty on Lifetime Assessments

Quantifying the impact of sputtering uncertainty on erosion estimates is complicated by the fact that the sputtering models are non-linear and the plasma properties are nonmonotonic. Indeed, in some cases (Fig. 3b), we have seen that the sputtering models can have uncertainty exceeding an order of magnitude and that the ion energy spectrum can exhibit values ranging from 0 to 300 eV (Fig. 8b). With that said, despite the variability in both sputtering yields and data, we generally have found that for a wide range of erosion rates (Figs. 9–12) the variance in the erosion predictions is only on the order of 190%.

One possible explanation for this relatively low variance stems from the wire geometry. The sputtering model with the largest uncertainty is the normal incidence for sputtering of gold. However, the gold-coated layer on the wires is relatively thin and in fact erodes very quickly at 18 and 33 deg from the thruster centerline. The

preponderance of erosion instead is the result of the sputtering of the underlying molybdenum. We thus may expect that the contribution to uncertainty from the gold erosion may not drastically impact the overall confidence. On the other hand, we see that the sputtering yields for normal incidence on molybdenum as well as for the angular sputtering yields all only have variances on the order of 150%. This level of uncertainty is commensurate with the uncertainty in erosion predictions we reported in the previous section.

With that said, while the gold layer is completely removed at most locations we consider, this surface does not completely erode at 63 deg from the thruster centerline. This location correspondingly exhibits higher relative uncertainty (greater than 150%), as we show in Fig. 13b for both angular incidence sputtering models. Because the gold layer is not completely eroded and the variance in the sputtering yield model for gold is larger than that of molybdenum (Fig. 3), we expect the relative uncertainty in the erosion to be high at this location. Another potential factor adding to the higher relative uncertainty at this angular location is the nonlinearity of the sputtering yield at low energies. We recall that at 63 deg from the thruster centerline, most of the ions have energies below 50 eV (Fig. 8b). These energies correspond to the highest variances in the gold sputtering yield model (Fig. 3b), as the sputtering yield is highly nonlinear near the threshold energy. Additionally, the variance in the threshold energy itself significantly changes the sputtering yield. While most ions at 63 deg can sputter gold if the threshold energy is 10 eV, most ions cannot sputter gold if the threshold energy increases to 30 eV.

In practice, our confidence in our erosion estimate suggests a potential guideline for wire design: adopting at least 190% in margin on the wire radius. This may be sufficient to mitigate the uncertainty in erosion prediction. Indeed, the fact that this 190% appears valid for a wide range of plasma conditions and erosion (Fig. 13b) further supports its adoption as a general guideline. With that said, we note that it is possible that our simulations and experiments may not have captured all representative conditions for a thruster on orbit. This may suggest that 190% is not a universally sufficient margin. We expand upon this in the following section.

### C. Sources of Uncertainty Beyond Sputtering Yield

While there are other sources of uncertainty that may impact the erosion estimates such as uncertainty in the local plasma properties, we have neglected these as small when compared to the order of magnitude variance in the sputtering yield. As we had a controlled experimental environment, we were confident in this assumption. This is borne out by the quantitative agreement of our model predictions with experiment. In practice, however, for making predictions of erosion on spacecraft surfaces in orbit, these plasma-based

uncertainties must be considered. This stems in large part from the fact that on-orbit measurements for the plasma environment are not available and that plume models for the space environment are limited [44]. Indeed, the ion energies and fluxes at the periphery of the plasma are highly susceptible to the background pressure in the test facility [45,46], and the variation in these properties with pressure is not well understood. This results in a large degree of uncertainty as to what these plume properties will be on orbit where the background pressure is absent. As the ion energies in the plume are closest to the regions of highest uncertainty in the sputtering yield (i.e., near the threshold energies), we anticipate that on-orbit predictions may be particularly susceptible to the variance in the sputtering yield models. With that said, this additional uncertainty can be incorporated into the formalism we have introduced here by treating the plasma properties as probabilistic as well and sampling over their distributions. This ultimately will be a critical step for fully quantifying the uncertainty in predictions for spacecraft component erosion in space.

#### D. Limitations of Erosion Model

While the results of the erosion model match the experimentally measured profiles well, our approach does have limited fidelity. For example, even though studies have shown that surface roughness can impact the sputtering yield by a factor of 2 [47], we have neglected this effect. This decision was largely motivated by the fact that reduced-fidelity, analytical models for this effect are still under investigation. With that said, our calibrated model does in some sense implicitly account for the uncertainty due to material surface conditions. As we discussed in Sec. III, the experimental conditions and properties of the target materials (such as roughness) used for generating the data sets varied across studies. This can in part explain the relatively large variance in sputtering yield as functions of both energy and angle. Our model inference method inherently accounts for this uncertainty in the calibration.

We have also neglected redeposition of sputtered material on the wires. As the wires in the mesh reflector coupons are close to each other, sputtered material from one wire could redeposit on an adjacent wire. Additionally, sputtered material could redeposit on the same wire. However, we expect the redeposition of material is small compared to the erosion of the wire.

Another limitation of our approach is that we only consider the effects of singly charged ions, neglecting the impact of charge-exchange neutral particles and multiply charged species. The expectation is that these higher-energy particles could lead to higher rates of erosion. Our modeling approach could be adapted to account for these higher-energy species by treating each charge species separately with its own associated current density in Eq. (1). This would require an estimate of the relative species concentration of each charge state. With that said, given the relatively large uncertainty in our erosion predictions (Fig. 9) as well as the relatively low fraction of higher charge states in Hall thrusters [43], this effect may be comparatively small.

Finally, we currently assume the ions impact the wire from one direction. Incorporating a two-dimensional ion velocity distribution would allow us to capture the differing flux of ions from different directions, giving a better estimate of erosion. In fact, using the ion velocity distribution would allow us to capture erosion around the entire wire; assuming the ions impact the wire from one direction gives no erosion on the side of the wire not facing the ions. We anticipate this effect would be relatively small close to the thruster centerline (less than 30 deg). The ions in this region are primarily moving in one direction because they have been accelerated by the axial electric field in the thruster. However, at the periphery of the plume, ions are largely formed by charge-exchange collisions with neutrals. The velocity of the neutrals is not influenced by the electric field, and the motion of the low-energy ions formed in charge-exchange collisions is susceptible to the local electric field. Therefore, we may expect at these periphery regions that the incident ions may not all originate from the thruster beam.

#### E. Recommendations for Improving Accuracy of Erosion Assessments

The central thesis of this work is that the uncertainty in sputtering yield models can translate to high degrees of uncertainty in sputtering erosion. To reduce the uncertainty in the eroded wire profiles, we thus need to reduce the uncertainty in the sputtering models. As we have discussed in the preceding section, some of the inherent uncertainty stems from the variance across data sets. This likely can be attributed to the varying experimental conditions that were employed for these disparate studies. Improved fidelity could be achieved by performing additional sputtering studies on material states (i.e., roughness) and under conditions that more accurately reflect the spacecraft surface.

The shapes of the median fits and credible intervals in Figs. 3 and 4 also suggest potential follow-up experiments that could be performed to improve model fidelity. For example, we see from Fig. 3b that there is a high degree of variability in the model fit for higher energies (exceeding 50 eV). This stems in large part from the fact that there are only data available at these higher energies where the underlying model (Eq. (3)) is relatively flat and not as easily constrained. The model uncertainty could be reduced by generating more data near the threshold energy (approximately 20 eV) where the underlying equation is more nonlinear. This points to the need for additional experiments to selectively target these lower energies for gold sputtering.

The model fits in the angular sputtering yields, Fig. 4, also would benefit from additional data, particularly for the sputtering yields for gold. However, we note that, with the exception of the Wei et al. model for molybdenum (Fig. 4b), the shape of the median fits and credible intervals for the angular model show qualitatively less agreement with the data. This suggests that the underlying physics-based models for the angular dependence may be missing key elements of the physical processes. Indeed, this variance may in large part be attributed to attempting to fit a functional shape that does not conform to the data. Ultimately, the reduced applicability of the model may not be surprising as the preponderance of sputtering yield data and models has been derived for higher energy levels (greater than 500 eV). Other physical phenomena may play a role at these lower energies. With this in mind, a more pressing recommendation for reducing uncertainty for the angular dependence is to revisit the underlying theory for the governing equations.

## VII. Conclusions

In summary, the goal of this work has been to quantify the impact of uncertainty in sputtering yield on predictions for erosion due to spacecraft interactions with the plume of a Hall effect thruster. This is a critical question, as the high-energy ions from this source can lead to component failure over time. Understanding the predicted erosion and being able to identify the margin for this erosion to guarantee spacecraft life are thus of practical interest. With this in mind, this work has investigated a model to predict the eroded profile of a key element for spacecraft: the gold-coated molybdenum rounded wires in mesh reflectors. This model discretizes the cross-section of the wire and takes inputs for the local current density, ion energy distribution, and sputtering yield to track how those discretized surfaces erode through time. To assess the impact of sputtering yield uncertainty on the erosion predictions, Bayesian inference was applied to determine the probability distributions for three known semi-empirical models for the sputtering yield of xenon on molybdenum and gold. Sampling from these distributions of the model parameters, the erosion model was ran 10,000 times to build statistical estimates for the wire erosion.

Experimental data for the plume of a 6 kW Hall thruster provided input plasma data for the erosion model [31]. The model predictions for erosion were compared to experimental measurements of wire samples. These samples were placed at four angles from the thruster centerline and 1 m downstream of the thruster. The eroded states varied from nearly complete erosion to only minor erosion on the wire surface layer, thus providing a varied data set for comparison. At all locations, the experimental measurements largely fell within the credible intervals for the predicted eroded wire profiles. In particular, at high erosion rates, the model was able to predict an unusual peak

like structure in the wire shape. This was attributed to the nonmonotonic dependence of angular sputtering on the incident angle.

In terms of the role of uncertainty, the largest relative uncertainty was in the regions of the plume where the energies are closest to the threshold energy for erosion. Because the gold is not completely eroded at this location, this may in part be explained by the lower confidence in the sputtering of gold compared to molybdenum. With that said, despite the fact that sputtering model uncertainty can vary by an order of magnitude, the confidence in erosion prediction only varied by 190%. This may in part be explained by the fact that at most locations examined the majority of the erosion occurs in the molybdenum substrate of the wire where sputtering is modeled with higher confidence.

This paper has discussed the results in the context of improving predictions for spacecraft erosion on orbit. In particular, these results would suggest that, despite the large variance in sputtering models at some energies and angles of incidence, for typical Hall thruster plumes, it may be sufficient to employ material margins with only 190% to ensure service life. The authors have qualified this conclusion with the understanding that the model does invoke a number of simplifying assumptions, such as the neglect of multiply charged species and surface roughness, and that in space the plasma conditions may trend more to the regions of higher uncertainty in the sputtering yields. This conclusion also holds for materials with similar levels of uncertainty in the sputter yield. Regardless, this work has established a rigorous framework for propagating and quantifying the role of sputtering uncertainty on erosion prediction. This is a critical, practical consideration for the design and margin choices of spacecraft components that may be subject to plume impingement.

## References

- [1] Oh, D. Y., Hastings, D. E., Marrese, C. M., Haas, J. M., and Gallimore, A. D., "Modeling of Stationary Plasma Thruster-100 Thruster Plumes and Implications for Satellite Design," *Journal of Propulsion and Power*, Vol. 15, No. 2, 1999, pp. 345–357.  
<https://doi.org/10.2514/2.5432>
- [2] Pencil, E. J., Randolph, T., and Manzella, D., "End-of-Life Stationary Plasma Thruster Far-Field Plume Characterization," *AIAA 32nd Joint Propulsion Conference*, AIAA Paper 1996-2709, 1996.
- [3] Randolph, T., Pencil, E., and Manzella, D., "Far-Field Plume Contamination and Sputtering of the Stationary Plasma Thruster," *AIAA 30th Joint Propulsion Conference*, AIAA Paper 1994-2855, 1994.
- [4] Oh, D. Y., and Hastings, D. E., "Three Dimensional PIC-DSMC Simulations of Hall Thruster Plumes and Analysis for Realistic Spacecraft Configurations," *32nd Joint Propulsion Conference and Exhibit*, AIAA Paper 1996-3299, 1996.  
<https://doi.org/10.2514/6.1996-3299>
- [5] Boyd, I. D., and Ketsdever, A., "Interactions Between Spacecraft and Thruster Plumes," *Journal of Spacecraft and Rockets*, Vol. 38, No. 3, 2001, pp. 380–380.  
<https://doi.org/10.2514/2.3712>
- [6] Likar, J. J., Bogorad, A., August, K. A., Lombardi, R. E., Kannenberg, K., and Herschitz, R., "Spacecraft Charging, Plume Interactions, and Space Radiation Design Considerations for All-Electric GEO Satellite Missions," *IEEE Transactions on Plasma Science*, Vol. 43, No. 9, 2015, pp. 3099–3108.  
<https://doi.org/10.1109/TPS.2015.2403272>
- [7] Inanaga, Y., and Muranaka, T., "Thruster Plume and Spacecraft Interaction Analysis by 3D Electrostatic Code for Hall Thruster," *36th International Electric Propulsion Conference*, Paper IEPC-2019-858, 2019, pp. 1–7.
- [8] Nuwal, N., Jambunathan, R., and Levin, D. A., "Kinetic Modeling of Spacecraft Surfaces in a Plume Backflow Region," *IEEE Transactions on Plasma Science*, Vol. 48, No. 12, 2020, pp. 4305–4325.  
<https://doi.org/10.1109/TPS.2020.3039110>
- [9] Yan, L., Wang, P. Y., Ou, Y. H., and Kang, X. L., "Numerical Study of Hall Thruster Plume and Sputtering Erosion," *Journal of Applied Mathematics*, Vol. 2012, Dec. 2012.  
<https://doi.org/10.1155/2012/3272021>
- [10] Sarraih, P., Hess, S. L., Mateo-Velez, J. C., Gineste, T., and Belhaj, M., "Simulations of Plasma Thruster Effect on the Electrostatic Behavior of Spacecrafts in GEO," *AIAA SPACE 2015 Conference and Exposition*, AIAA Paper 2015-4640, 2015, pp. 1–13.  
<https://doi.org/10.2514/6.2015-4640>
- [11] Corey, R. L., Gascon, N., Delgado, J. J., Gaeta, G., Munir, S., and Lin, J., "Performance and Evolution of Stationary Plasma Thruster Electric Propulsion for Large Communications Satellites," *28th AIAA International Communications Satellite Systems Conference, ICSSC 2010*, AIAA Paper 2010-8688, Sept. 2010, pp. 1–20.  
<https://doi.org/10.2514/6.2010-8688>
- [12] Hu, S. H., Joshi, A., Khayms, V., Emgushov, B., Werthman, L., and Smentkowski, V. S., "Hall Thruster Plume Effects and Sputtering of Spacecraft Surfaces," *37th Joint Propulsion Conference and Exhibit*, AIAA Paper 2001-3356, 2001.  
<https://doi.org/10.2514/6.2001-3356>
- [13] Young, J. A., Crofton, M. W., Glogowski, M., and Eskenazi, M., "Ageing Effects of a Hall Thruster Plume on Solar Array Performance and ESD Susceptibility," *35th International Electric Propulsion Conference*, Paper IEPC-2017-493, 2017.
- [14] Kannenberg, K., Khayms, V., Emgushov, B., Werthman, L., and Pollard, J. E., "Validation of Hall Thruster Plume Sputter Model," *37th Joint Propulsion Conference and Exhibit*, AIAA Paper 2001-3986, 2001.  
<https://doi.org/10.2514/6.2001-3986>
- [15] Bermúdez, L. M., Barnhart, K. J., Agathon-Burton, C. A., Basak, D., and Glogowski, M. J., "A Comprehensive Numerical Approach to the Modeling and Simulation of Plume Interaction Effects on Solar Electric Propulsion Spacecraft," *35th International Electric Propulsion Conference*, Paper IEPC-2017-238, 2017, pp. 1–14.
- [16] Zhang, Z., Zhang, Z., Tang, H., Liang Ling, W. Y., Chen, Z., Ren, J., and Cao, J., "Measurement of the Distribution of Charge Exchange Ions in a Hall-Effect Thruster Plume," *Plasma Sources Science and Technology*, Vol. 29, No. 8, 2020.  
<https://doi.org/10.1088/1361-6595/aba12c>
- [17] Noushkam, N., Basak, D., Glogowski, M., Crofton, M., Young, J., and Plecque, B., "Sputtering Effects of Xenon Ion Thruster Plume on Common Spacecraft Materials," *AIAA SPACE 2015 Conference and Exposition*, AIAA Paper 2015-4642, 2015, pp. 1–12.  
<https://doi.org/10.2514/6.2015-4642>
- [18] Eckstein, W., and Preuss, R., "New Fit Formulae for the Sputtering Yield," *Journal of Nuclear Materials*, Vol. 320, No. 3, 2003, pp. 209–213.  
[https://doi.org/10.1016/S0022-3115\(03\)00192-2](https://doi.org/10.1016/S0022-3115(03)00192-2)
- [19] Yamamura, Y., and Shindo, S., "An Empirical Formula for Angular Dependence of Sputtering Yields," *Radiation Effects*, Vol. 80, Nos. 1–2, 1984, pp. 57–72.  
<https://doi.org/10.1080/00337578408222489>
- [20] Wei, Q., Li, K.-D., Lian, J., and Wang, L., "Angular Dependence of Sputtering Yield of Amorphous and Polycrystalline Materials," *Journal of Physics D: Applied Physics*, Vol. 41, No. 17, 2008, Paper 172002.  
<https://doi.org/10.1088/0022-3727/41/17/172002>
- [21] Rosenberg, D., and Wehner, G. K., "Sputtering Yields for Low Energy He<sup>+</sup>, Kr<sup>+</sup>, and Xe<sup>+</sup>-Ion Bombardment," *Journal of Applied Physics*, Vol. 33, No. 5, 1962, pp. 1842–1845.  
<https://doi.org/10.1063/1.1728843>
- [22] Zalm, P. C., "Energy Dependence of the Sputtering Yield of Silicon Bombarded with Neon, Argon, Krypton, and Xenon Ions," *Journal of Applied Physics*, Vol. 54, No. 5, 1983, pp. 2660–2666.  
<https://doi.org/10.1063/1.332340>
- [23] Doerner, R. P., Whyte, D. G., and Goebel, D. M., "Sputtering Yield Measurements During Low Energy Xenon Plasma Bombardment," *Journal of Applied Physics*, Vol. 93, No. 9, 2003, pp. 5816–5823.  
<https://doi.org/10.1063/1.1566474>
- [24] Kolasinski, R. D., "Oblique Angle Sputtering Yield Measurements for Ion Thruster Grid Materials," *41st AIAA/ASME/SAE/ASEE Joint Propulsion Conference and Exhibit*, AIAA Paper 2005-3526, July 2005, pp. 1–16.  
<https://doi.org/10.2514/6.2005-3526>
- [25] Duchemin, O. B., and Polk, J. E., "Low Energy Sputtering Experiments for Ion Engine Lifetime Assessment," *35th Joint Propulsion Conference and Exhibit*, AIAA Paper 1999-2858, 1999.  
<https://doi.org/10.2514/6.1999-2858>
- [26] Rubin, B., Topper, J. L., Farnell, C. C., and Yalin, A. P., "Quartz Crystal Microbalance-Based System for High-Sensitivity Differential Sputter Yield Measurements," *Review of Scientific Instruments*, Vol. 80, No. 10, 2009, pp. 103506–103509.  
<https://doi.org/10.1063/1.3249560>
- [27] Tondou, T., Inguibert, V., Darnon, F., and Roussel, J. F., "Angular Characterisation of Erosion and Contamination by Electric Propulsion," *4th International Spacecraft Propulsion Conference*, Paper 2004ESASP.55E.105T, 2004.
- [28] Tartz, M., Heyn, T., Bundesmann, C., Zimmermann, C., and Neumann, H., "Sputter Yields of Mo, Ti, W, Al, Ag under Xenon Ion Incidence,"

- European Physical Journal D*, Vol. 61, No. 3, 2011, pp. 587–592.  
<https://doi.org/10.1140/epjd/e2010-10553-8>
- [29] Yim, J. T., “A Survey of Xenon Ion Sputter Yield Data and Fits Relevant to Electric Propulsion Spacecraft Integration,” *35th International Electric Propulsion Conference*, Paper IEPC-2017-060, 2017.
- [30] Meyer, M. E., Byrne, M. P., Jorns, B. A., and Boyd, I. D., “Erosion of a Meshed Reflector in the Plume of a Hall Effect Thruster, Part 1: Modeling,” *AIAA Propulsion and Energy 2019 Forum*, AIAA Paper 2019-3987, 2019.  
<https://doi.org/10.2514/6.2019-3987>
- [31] Byrne, M. P., Meyer, M. E., Boyd, I. D., and Jorns, B. A., “Erosion of Meshed Reflector in the Plume of a Hall Effect Thruster, Part 2: Experiments,” *AIAA Propulsion and Energy 2019 Forum*, AIAA Paper 2019-3988, 2019.  
<https://doi.org/10.2514/6.2019-3988>
- [32] Jorns, B., and Byrne, M., “Model for the Dependence of Cathode Voltage in a Hall Thruster on Facility Pressure,” *Plasma Sources Science and Technology*, Vol. 30, No. 1, 2021, Paper 015012.  
<https://doi.org/10.1088/1361-6595/abd3b6>
- [33] Saravia, M., Giacobbe, A., and Andreussi, T., “Bayesian Analysis of Triple Langmuir Probe Measurements for the Characterization of Hall Thruster Plasmas,” *Review of Scientific Instruments*, Vol. 90, No. 2, 2019, Paper 023502.  
<https://doi.org/10.1063/1.5079532>
- [34] Byrne, M. P., and Jorns, B. A., “Data-Driven Models for the Effects of Background Pressure on the Operation of Hall Thrusters,” *Proceedings of the 36th International Electric Propulsion Conference*, Paper IEPC-2019-630, 2019, pp. 15–20.
- [35] Ikuse, K., Yoshimura, S., Hine, K., Kiuchi, M., and Hamaguchi, S., “Sputtering Yields of Au by Low-Energy Noble Gas Ion Bombardment,” *Journal of Physics D: Applied Physics*, Vol. 42, No. 13, 2009.  
<https://doi.org/10.1088/0022-3727/42/13/135203>
- [36] Bohdansky, J., “A Universal Relation for the Sputtering Yield of Monatomic Solids at Normal Ion Incidence,” *Nuclear Instruments and Methods in Physics Research, B*, Vol. 2, No. 1, 1984, pp. 587–591.  
[https://doi.org/10.1016/0168-583X\(84\)90271-4](https://doi.org/10.1016/0168-583X(84)90271-4)
- [37] Sivia, D., and Skilling, J., *Data Analysis: A Bayesian Tutorial*, Oxford Univ. Press, Oxford, 2006.
- [38] McDonald, M. S., and Gallimore, A. D., “Cathode Position and Orientation Effects on Cathode Coupling in a 6-kW Hall Thruster,” *31st International Electric Propulsion Conference*, Paper IEPC-2009-113, 2009.
- [39] Brown, D. L., “Investigation of Low Discharge Voltage Hall Thruster Characteristics and Evaluation of Loss Mechanisms,” Ph.D. Dissertation, Univ. of Michigan, Ann Arbor, MI, 2009.
- [40] Reid, B. M., “The Influence of Neutral Flow Rate in Operation of Hall Thrusters,” Ph.D. Dissertation, Univ. of Michigan, Ann Arbor, MI, 2009.
- [41] McDonald, M. S., “Electron Transport in Hall Thrusters,” Ph.D. Dissertation, Univ. of Michigan, Ann Arbor, MI, 2012.
- [42] Hofer, R. R., “Development and Characterization of High-Efficiency, High-Specific Impulse Xenon Hall Thrusters,” Ph.D. Dissertation, Univ. of Michigan, Ann Arbor, MI, 2004.
- [43] Goebel, D. M., and Katz, I., *Fundamentals of Electric Propulsion: Ion and Hall Thrusters*, Wiley, New York, 2008.
- [44] Laube, J., Massaccesi, N., Zitouni, B., and Peukert, M., “EP Plasma Plume in Orbit: Diagnostics and Analysis Correlation,” *36th International Electric Propulsion Conference, IEPC-2019-294*, 2019.
- [45] Huang, W., Kamhawi, H., and Haag, T., “Facility Effect Characterization Test of NASA’s HERMeS Hall Thruster,” *52nd AIAA/SAE/ASEE Joint Propulsion Conference*, AIAA Paper 2016-4828, 2016.  
<https://doi.org/10.2514/6.2016-4828>
- [46] Brown, D. L., Walker, M. L., Szabo, J., Huang, W., and Foster, J. E., “Recommended Practice for Use of Faraday Probes in Electric Propulsion Testing,” *Journal of Propulsion and Power*, Vol. 33, No. 3, 2017, pp. 582–613.  
<https://doi.org/10.2514/1.B35696>
- [47] Kuestner, M., Eckstein, W., Dose, V., and Roth, J., “The Influence of Surface Roughness on the Angular Dependence of the Sputter Yield,” *Nuclear Instruments and Methods in Physics Research Section B: Beam Interactions with Materials and Atoms*, Vol. 145, No. 3, 1998, pp. 320–331.  
[https://doi.org/10.1016/S0168-583X\(98\)00399-1](https://doi.org/10.1016/S0168-583X(98)00399-1)

A. D. Ketsdever  
 Associate Editor